frontiers | Frontiers in Molecular Neuroscience

TYPE Original Research
PUBLISHED 03 June 2025
DOI 10.3389/fnmol.2025.1574219



OPEN ACCESS

EDITED BY
Volker Eulenburg,
University of Augsburg, Germany

REVIEWED BY
Johannes Oberwinkler,
University of Marburg, Germany
Myeounghoon Cha,
Soonchunhyang University, Republic of Korea

*CORRESPONDENCE
Max Larsson
✉ max.larsson@liu.se

RECEIVED 10 February 2025
ACCEPTED 12 May 2025
PUBLISHED 03 June 2025

CITATION
Chen JCY, Kaczmarczyk L, Jackson WS and Larsson M (2025) A $Na_V1.8^{FlpO}$ mouse enabling selective intersectional targeting of low threshold C fiber mechanoreceptors and nociceptors.
*Front. Mol. Neurosci.* 18:1574219.
doi: 10.3389/fnmol.2025.1574219



# A $Na_V1.8^{FlpO}$ mouse enabling selective intersectional targeting of low threshold C fiber mechanoreceptors and nociceptors

John C. Y. Chen[1], Lech Kaczmarczyk[1,2], Walker S. Jackson[1,2] and Max Larsson[1]*

[1]Division of Cell-and Neurobiology, Department of Biomedical and Clinical Sciences, Linköping University, Linköping, Sweden, [2]Wallenberg Center for Molecular Medicine, Linköping University, Linköping, Sweden

Genetic targeting of select populations of cells in the mouse nervous system is often hampered by a lack of selectivity, as candidate genes for such targeting are commonly expressed by multiple cell populations, also in the same region. Intersectional targeting using two or more genes has been enabled by the development of reporter tools dependent on more than one recombinase or gene regulator. Still, widespread adoption of intersectional tools is complicated by a scarcity of driver mice expressing recombinases other than Cre. Here we report the generation and characterization of a new driver mouse that expresses the FlpO recombinase from the endogenous locus of the *Scn10a* gene encoding $Na_V1.8$, a voltage-gated sodium channel that is almost exclusively expressed in the afferent limb of the peripheral nervous system. Moreover, among sensory neurons the channel is preferentially expressed in nociceptors and in low-threshold C-fiber mechanoreceptors (C-LTMRs). The mouse showed high recombination efficiency (97%) and selectivity (93%) in dorsal root ganglia. Reporter-expressing fibers were observed in a variety of peripheral tissues, including skin, skeletal muscle, genitalia, bladder and intestines. To validate the suitability of the FlpO mouse line for intersectional targeting, we crossed it with a mouse line expressing CreERT2 from the *Th* (tyrosine hydroxylase) locus. This approach resulted in strikingly selective and efficient targeting of C-LTMRs, showing robust visualization of nerve endings of these fibers in skin and spinal cord at the light and electron microscopic level. Thus, the $Na_V1.8^{Flpo}$ mouse line presented here constitutes a selective and versatile tool for intersectional genetic targeting of $Na_V1.8$ expressing primary afferent neurons.

KEYWORDS

**pain, nociception, somatosensory system, primary afferent fibers, spinal cord, APEX2**

## Introduction

Primary afferent fibers innervating skin and internal organs are pivotal for sensing the external and internal environments, thus informing behavior and homeostasis that enable the survival of the organism. Such sensory fibers include low-threshold mechanoreceptors (LTMRs) that signal innocuous mechanical stimuli, as well as nociceptors that are activated by noxious stimuli that threaten the integrity of the tissue. The last decade has seen a rapid progress in delineating primary afferent populations via transcriptomics and other means,

identifying genetic markers of such populations (e.g., Kupari and Ernfors, 2023; Sharma et al., 2020; Usoskin et al., 2015; Handler and Ginty, 2021; Li et al., 2015). However, whereas in some cases this has allowed targeting of relatively homogeneous populations for functional and anatomical characterization using Cre-expressing mouse lines (Qi et al., 2024b; Li et al., 2011), such an approach is often hampered by the lack of a single genetic marker that uniquely identifies the population of interest.

C fiber low-threshold mechanoreceptors (C-LTMRs) are thought to mediate pleasant touch (Löken et al., 2009; Olausson et al., 2002; Huzard et al., 2022) but have also been suggested to have a role in pain modulation (Larsson and Nagi, 2022). However, investigation of the function of these fibers in animals has been hindered by a lack of genetic tools for selective functional manipulation. C-LTMRs express *Th* (encoding tyrosine hydroxylase, TH) and *Slc17a8* (encoding the vesicular glutamate transporter 3, VGluT3); however, those genes are also expressed in other cells in the CNS and peripheral tissue, which complicates the use of mice expressing Cre or tamoxifen-inducible CreERT2 from the loci of either of these genes. For instance, targeting of a genetically encoded actuator protein using $Th^{CreERT2}$ mice may also capture mechanosensitive Merkel cells in the skin (Hoffman et al., 2018), sympathetic nerve fibers, as well as catecholaminergic neurons in the brainstem. However, unlike those cells, C-LTMRs also express the voltage-sensitive sodium channel $Na_V1.8$, encoded by the gene *Scn10a*. Thus, it may be possible to employ an intersectional targeting approach that uses $Th^{CreERT2}$ driver mice together with a second driver mouse line expressing a distinct recombinase from the *Scn10a* locus, in combination with double recombinase dependent genetic tools. Moreover, in addition to C-LTMRs, $Na_V1.8$ is selectively expressed in most nociceptors whereas myelinated LTMRs have little or no expression of this ion channel. A $Na_V1.8$ driver mouse could therefore potentially be used for intersectional targeting of nociceptor subpopulations where the second genetic marker is not nociceptor-specific. We therefore generated a new mouse line that expresses FlpO recombinase from the *Scn10a* locus and explored its utility for targeting of $Na_V1.8$-expressing primary afferent neurons in somatosensory and viscerosensory pathways, including intersectional selective targeting of C-LTMRs.

# Materials and methods

## Gene targeting

The $Na_V1.8^{FlpO}$ knock-in mouse line was generated through homologous recombination in J1 embryonic stem cells (derived from 129S4 mice) at the Karolinska Center Transgene Technology. The *Scn10a*-IRES2-FlpO targeting vector (TV) was constructed using the Gibson Assembly cloning kit (New England Biolabs). The IRES2-FlpO cassette was inserted 10 base pairs downstream of the stop codon of the last $Na_V1.8$ exon. The vector incorporated a self-excision tACE-Cre-Neo (ACN) selection cassette, similar to the design originally described by Bunting et al. (1999), but with Lox2272 flanking sites. After excision, a single lox site remained 19 base pairs downstream of the terminal exon. The plasmid containing the ACN cassette was kindly provided by Mario Capecchi (Addgene plasmid #20343; Wu et al., 2008). Homology arms for the targeting vector were amplified via PCR from mouse ES cell DNA using the following primers: Forward: CCCGTGTGCCAGGA ACTGAGTC Reverse: CATCAACTCATGCTTGGATGGTGT. The vector backbone was based on the Slc1a3-CreERT2 plasmid (Addgene plasmid #129409; Kaczmarczyk et al., 2021), linearized with AscI and SmaI restriction enzymes. To enhance homologous recombination efficiency, the TV was co-electroporated with a pX330-Nav1.8 Cas9 vector containing a suitable sgRNA sequence (ATGCTGGAG TGTCTTCACTG). The pX330 backbone was a gift from Feng Zhang (Addgene plasmid #42230; Cong et al., 2013). The full sequences of both the TV and the Cas9 plasmid are available at https://tinyurl.com/Scn10a-IRES2-FlpO. Plasmid integrity was verified by restriction digest and Sanger sequencing. As a result of successful gene targeting, the *Scn10a* locus encoding $Na_V1.8$ was replaced with an *Scn10a*-IRES2-FlpO-3'UTR cassette (Figure 1A).

## Animals

For Flp-dependent reporter expression, $Na_V1.8^{FlpO}$ mice were crossed with Ai65F mice (RCF-tdT; Jackson Laboratory, strain #032864) (Daigle et al., 2018). For intersectional genetic targeting of C-LTMRs, $Na_V1.8^{FlpO}$ mice were crossed with either Ai65 mice (RCFL-tdT; Jackson Laboratory, strain #021875) (Daigle et al., 2018) or ROSA26DR-Matrix-dAPEX2 (Jackson Laboratory, strain #032764; here called APEX2 mice) (Zhang et al., 2019); the resulting offspring was further crossed with $Th^{CreERT2}$ mice (Jackson Laboratory, strain #025614) (Abraira et al., 2017) to generate offspring heterozygous for $Na_V1.8^{FlpO}$, $Th^{CreERT2}$, and reporter. $Th^{CreERT2}$ mice were also crossed with singly Cre-dependent Ai14 mice (RCL-tdTomato, Jackson Laboratory, strain #007914) (Madisen et al., 2010). Mouse genotyping was performed using the following primers: wt forward, 5'-CTG AGG GTC GGC CAT TAA AAT TGA-3′; mutant forward, 5'-ACC TGA GGG TCG GCC ATT AAA ATT GA-3′; wt reverse, 5′-GAG ATT GAC CTC YGG CCT CCA AA-3′; mutant reverse, 5'CAG AGA TTG ACC TCT GGC CTC CAA A-3′. All animal experiments were approved by the Animal Ethics Committee at Linköping University (permits no. 2439–2021 and 214–2021) and performed in accordance with the EU Directive 2010/63/EU.

## Behavioral assays

To assess potential effects of the modified *Scn10a* allele on acute nociception, 6–8 week old homozygous $Na_V1.8^{Flpo/FlpO}$ mice (4 females, 4 males) and wildtype C57BL/6Jrj mice (4 females, 3 males) were subjected to von Frey and hot plate assays. For the von Frey assay, mice were placed in a small plexiglass cubicle (W × D × H 9 × 5 × 5 cm) with a mesh floor. After 15 min habituation, the mechanical paw withdrawal threshold was assessed using manual von Frey filaments applied to the plantar hindpaw. The mechanical von Frey threshold was determined using the simplified up-down method (Bonin et al., 2014). The hot plate assay was performed using a hot plate analgesia meter (IITC Life Science). The mouse was put on the hot plate set to a constant temperature of 50°C, and immediately removed when jumping or paw licking/flicking was observed. Each mouse underwent three trials (minimum 15 min inter-trial interval) and the average latency to nocifensive behavior calculated.

10.3389/fnmol.2025.1574219

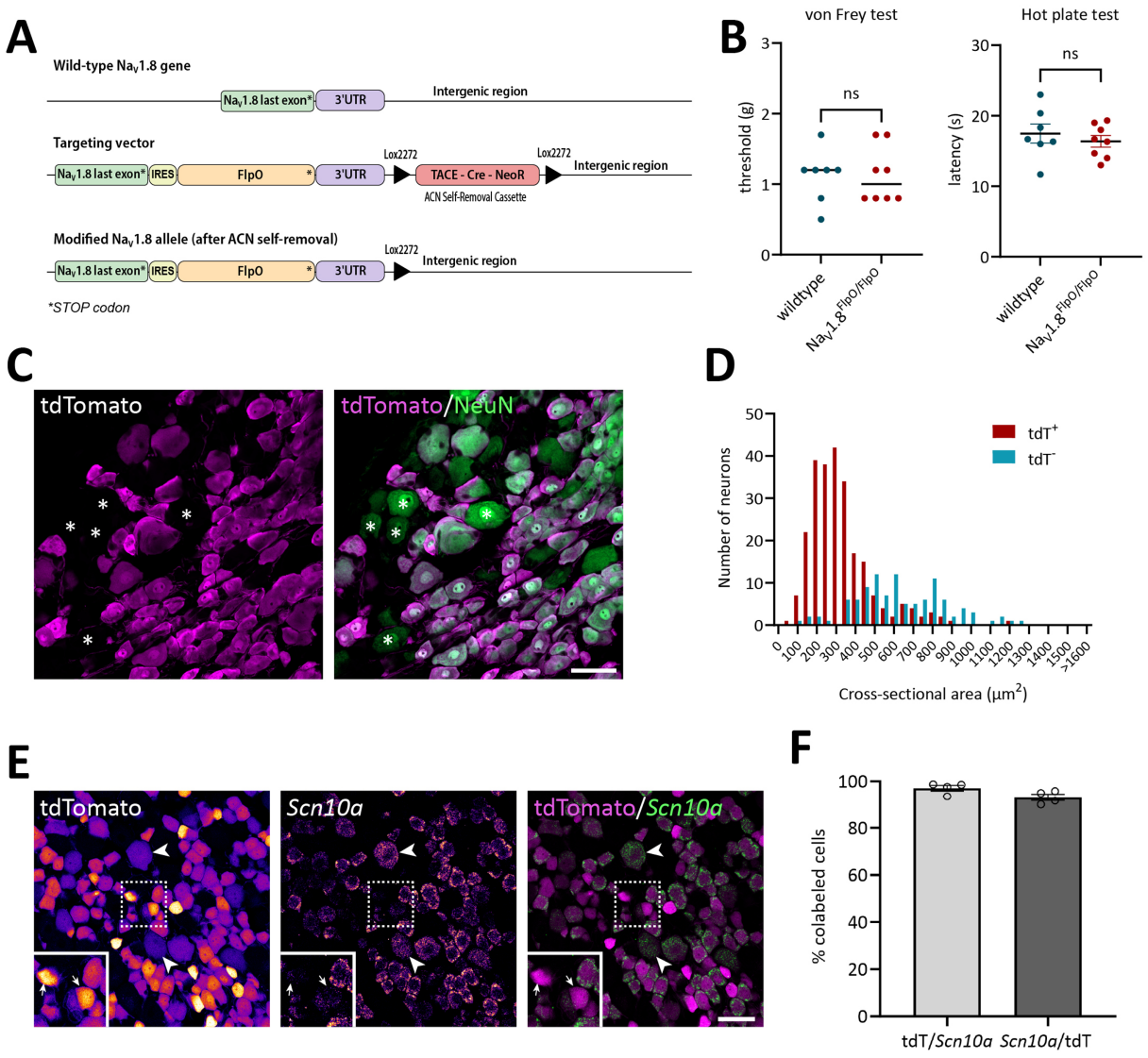


FIGURE 1
Verification of the Na$_V$1.8$^{FlpO}$ mouse line. **(A)** Gene targeting strategy. To drive the expression of FlpO from the gene encoding Na$_V$1.8 without interfering with its expression, a targeting vector was engineered with a cassette carrying an internal ribosome entry site (IRES) and FlpO inserted 10 base pairs downstream of the endogenous stop codon. A floxed Neomycin resistance selectable marker (TACE-Cre_NeoR) was placed downstream of the gene. Upon passage of the allele through the male germline, testes-specific expression of Cre recombinase led to the removal of the selectable marker. The final modified allele has an IRES and FlpO immediately downstream of the native stop codon and a single Lox2272 sequence downstream of the gene. **(B)** von Frey and hot plate assays to probe potential effects on acute mechanical and heat nociception in NaV1.8FlpO homozygous mice compared to wildtype C57BL/6Jrj mice. No significant genotype effects were found; *p* values are indicated in the graphs (left panel, two-tailed Mann–Whitney's exact test; right panel, two-tailed Student's t-test). Error line in the left panel indicates median; error bars in the right panel indicate mean ± S.E.M. Each data point indicates results from a single animal. *n* = 8 Na$_V$1.8$^{FlpO/FlpO}$ mice (4 females), *n* = 7 C57BL6/Jrj mice (4 females). **(C)** Expression of tdTomato in NeuN$^+$ neurons in a lumbar DRG of a Na$_V$1.8$^{Flpo}$;Ai65F mouse. Single optical section, 20x/0.8 objective, pinhole 32 µm. **(D)** Size histogram of tdTomato$^+$ and tdTomato$^-$ DRG neurons. *n* = 3 mice (one section and ganglion per mouse). **(E)** Co-localization of tdTomato immunofluorescence with *Scn10a* transcript detected using *in situ* hybridization in a lumbar DRG. Single optical section, 20x/0.8 objective, pinhole 37 µm. Left and middle panels show tdTomato immunofluorescence and *Scn10a in situ* hybridization separately, pseudo-colored using the Fire look-up table in Fiji to enhance visibility. Examples of weakly tdTomato immunoreactive (IR) cells are indicated by arrowheads, while arrows in inset show examples of tdTomato-IR cells with low levels of *Scn10a* transcript. Dashed frame indicates the region magnified in the inset. **(F)** Recombination efficiency with respect to *Scn10a*$^+$ cells (mean ± S.E.M.) in L3-L5 DRGs. Each data point indicates a section from a single ganglion; *n* = 3 mice. Scale bars in B and D, 50 µm.

## Tamoxifen injection

For *Th*$^{CreERT2}$; Na$_V$1.8$^{FlpO}$; Ai65 and *Th*$^{CreERT2}$; Na$_V$1.8$^{FlpO}$; APEX2 mice, tamoxifen (T5648, Sigma-Aldrich) dissolved in corn oil at a concentration of 20 mg/mL was administered at 8–10 weeks of age by a single injection (100 µL, i.p.). The mice were perfused no earlier than 2 weeks after injection.

## Tissue preparation

Adult mice of either sex were anesthetized with i.p. injections of either sodium pentobarbital (100 mg/kg) or a mixture of ketamine (120 mg/kg) and dexmedetomidine (0.5 mg/kg), after which they were subjected to transcardial perfusion using 5 mL phosphate buffer (PB, 0.1 M pH 7.4) followed by 50 mL of 4% paraformaldehyde (for

immunofluorescence) or 2% paraformaldehyde and 2.5% glutaraldehyde (for electron microscopy). Tissue of interest was harvested, post-fixed overnight at 4°C and then stored in 1/10 fixative or PB until further processing.

## Immunofluorescence

Tissue specimens were cryoprotected in 30% sucrose, embedded in OCT, cut at 15 µm or 50 µm thickness in a cryostat and placed on glass slides. Alternatively, specimens were embedded in 4% low-melting agarose and cut on a vibrating microtome (Campden Instruments 7,000smz-2) at 50 µm thickness. Sections were incubated in phosphate-buffered saline (PBS) with 3% normal goat serum, 0.5% bovine serum albumin and 0.5% Triton X-100 (blocking solution), and then in blocking solution with primary antibodies (see Table 1) overnight at room temperature. Sections were next rinsed and incubated in secondary antibody solution (Table 2). For detection of isolectin $B_4$ ($IB_4$) binding sites, biotinylated $IB_4$ (Life Technologies, I21214) was added to the primary antibody solution at 1:1,000 dilution, and streptavidin-Alexa Fluor 488 (Life Technologies, S11223) added to the secondary antibody solution at 1:500 dilution. In some cases, cell nuclei were stained using DAPI or SYTOX Deep Red (ThermoFisher Scientific, S11380). Sections were coverslipped with Prolong Diamond, Prolong Glass or SlowFade Diamond (Life Technologies) and imaged using Zeiss LSM800 (10x/0.3, 20x/0.8, 40x/1.3 and 63x/1.4 objectives), Leica Stellaris 5 (63x/1.4 objective) confocal microscopes, or Leica DMi8 epifluorescence microscope (20x/0.5 objective, for tile scans of parasagittal brain sections and spinal cord overviews).

## *In situ* hybridization

The *in situ* hybridization chain reaction (HCR) protocol was based on Molecular Instruments' HCR RNA-FISH protocol for frozen fixed tissue sections. DRG cryostat sections (15 µm thickness) were incubated in probe hybridization buffer with 0.4 pmol of each probe set overnight at 37°C, after which the sections were washed using probe wash buffer and 5X SSCT (sodium chloride sodium citrate with 0.1% Tween 20). Before amplification, 6 pmol of hairpin h1 and 6 pmol of hairpin h2 were denatured (95°C for 90 s, followed by cooling at room temperature in the dark for 30 min). The sections were then incubated in amplication buffer with the h1 and h2 hairpins overnight at room temperature, and then washed in 5X SSCT to remove excess hairpins. After coverslipping with Prolong Diamond, the sections were imaged in a Zeiss LSM800 confocal microscope.

## Electron microscopy

The day after perfusion fixation, thoracic spinal cord from three $Th^{CreERT2}$; $Na_V1.8^{FlpO}$; APEX2 mice was embedded in 4% low-melting agarose, cut on a vibrating microtome into 50 µm or 150 µm

TABLE 1 Primary antibodies.

| Antigen | Host, isotype | Supplier | Cat # | Dilution |
|---|---|---|---|---|
| CGRP | Guinea pig | Synaptic Systems | 414004 | 1:1000 |
| NFH | Chicken | Thermo Fisher Scientific | PA1-10002 | 1:1000 |
| NeuN | Mouse, $IgG_1$ | Merck Millipore | MAB377 | 1:1000 |
| Parvalbumin | Guinea pig | Synaptic Systems | 195004 | 1:500 |
| PKCγ | Guinea pig | Frontier Institute | PKCg-GP-Af350 | 1:250 |
| RFP (tdTomato) | Chicken | Synaptic Systems | 409006 | 1:2,000 |
| RFP (tdTomato) | Rabbit | Rockland | 600-401-379 | 1:1,000 |
| TH | Rabbit | Abcam | Ab112 | 1:200 |
| TRPV1 | Rabbit | Synaptic Systems | 444033 | 1:1,000 |
| VGluT3 | Guinea pig | Frontier Institute | VGLUT3-GP-Af300 | 1:500 |
| Vimentin | Mouse, $IgG_1$ | Santa Cruz | sc-6260 | 1:200 |

TABLE 2 Secondary antibodies.

| Host, target | Fluorophore | Supplier | Cat # | Dilution |
|---|---|---|---|---|
| Goat α-chicken IgY (H + L) | Alexa Fluor 488 | Life Technologies | A32931 | 1:500 |
| Goat α-chicken IgY (H + L) | Alexa Fluor 555 | Life Technologies | A21437 | 1:500 |
| Goat α-guinea pig IgG (H + L) | Alexa Fluor 488 | Life Technologies | A11073 | 1:500 |
| Goat α-guinea pig IgG (H + L) | Alexa Fluor 647 | Life Technologies | A21450 | 1:500 |
| Goat α-mouse $IgG_1$ | Alexa Fluor 488 | Life Technologies | A21121 | 1:500 |
| Goat α-rabbit IgG (H + L) | Alexa Fluor 488 | Life Technologies | A11034 | 1:500 |
| Goat α-rabbit IgG (H + L) | Alexa Fluor Plus 555 | Life Technologies | A32732 | 1:500 |

transverse sections, and immediately subjected to APEX2 histochemistry. The sections were incubated in 3,3′-diaminobenzidine (DAB) without $H_2O_2$ for 30–60 min, and then in DAB with $H_2O_2$ (Vector Laboratories SK-4100) for 45–60 min. The sections were then osmicated in 1% $OsO_4$ in 0.1 M PB, stained with 1% uranyl acetate in 70% ethanol, dehydrated in a graded series of ethanol and embedded in Durcupan. Ultrathin sections were placed on Formvar coated single-slot copper grids, counterstained with 2% aqueous uranyl acetate and 0.5% lead citrate (in some cases post-embedding counterstaining was omitted) and examined in a JEOL JEM1400 Flash transmission electron microscope at 80 kV accelerating voltage.

## Image analysis

To measure the soma size of DRG neurons, complete z-stacks (16–22 optical sections at 0.53 µm separation, 24 µm pinhole) of each DRG section were obtained using a Zeiss LSM800 confocal microscope and a 20x/0.8 objective, and analyzed using Fiji. The maximal cross-sectional area of each DRG neuron in the z-stack was determined. Neurons where the largest cross-sectional area was observed in the first or last optical section of the z-stack were excluded.

## Statistical analysis

All descriptive statistics and statistical tests were performed in GraphPad Prism. Parametric tests were performed only when the underlying data passed the Shapiro–Wilk normality test. All measures are given as mean ± S.E.M.

# Results

Mice heterozygous or homozygous for the *Scn10a*-IRES2-*FlpO* allele were viable, fertile and showed no overt behavioral deficits. Further, homozygous $Na_V1.8^{FlpO/FlpO}$ mice did not show any impairment with respect to mechanical nociceptive withdrawal reflexes or heat-induced nocifensive behavior (Figure 1B). In lumbar DRGs of $Na_V1.8^{FlpO}$; Ai65F mice, tdTomato protein was found in numerous NeuN immunoreactive neurons. Whereas the majority of tdTomato$^+$ neurons were small, some were medium-to-large sized (Figures 1C,D). In some immunolabeling experiments of the DRG, we noted enrichment of tdTomato immunolabeling at the plasma membrane of some neurons. This labeling pattern was only observed when using a rabbit anti-tdTomato antibody, not when using a chicken primary antibody, and was continuous with a gradient of immunolabeling into the cytosol of the neuron. Nevertheless, to rule out that this edge labeling represented tdTomato expression in satellite glial cells that surround DRG neurons, we co-immunolabeled for tdTomato and the satellite glial cell marker vimentin (Supplementary Figure S1). Indeed, no co-localization of tdTomato with vimentin was observed, confirming that tdTomato expression was restricted to neurons in the DRG. *In situ* hybridization showed that the vast majority (97.1 ± 1.2%) of *Scn10a*$^+$ neurons expressed tdTomato protein; conversely, 93.1 ± 1.4% of tdTomato$^+$ cells expressed *Scn10a* mRNA (Figures 1E,F) (here and elsewhere, mRNA is referred to by the gene name in italics, while protein names are written in regular font style). Calcitonin gene-related peptide (CGRP), $IB_4$ binding, and TRPV1 were found in subsets of tdTomato$^+$ neurons (Figure 2). tdTomato also showed partial overlap with neurofilament heavy chain (NFH) and its transcript *Nefh*, including in peripheral axons of the sciatic nerve. In the spinal cord, tdTomato$^+$ processes, i.e., presumed central projections of $Na_V1.8^+$ primary afferent fibers, were present throughout the dorsal horn at varying densities (Figure 3). The largest density of tdTomato$^+$ processes was found in lamina I and the dorsal half of lamina II, whereas ventral lamina II and dorsal lamina III, as outlined by the presence of PKC$\gamma^+$ neurons, showed a progressively lower density of processes along the dorsoventral axis. Processes were at all spinal levels considerably sparser in ventral lamina III to lamina V, and absent from the intermediate or ventral horns. Cell bodies exhibiting tdTomato fluorescence were not observed in the spinal cord. In spinal white matter, processes were found in Lissauer's tract as well as in the dorsal and medial parts of the dorsal funiculus. We did not attempt a comprehensive mapping of the distribution of tdTomato$^+$ cells and processes in the brain. However, tdTomato$^+$ structures were generally sparse (Figure 4). In the brainstem, tdTomato$^+$ processes were found in the trigeminal spinal nucleus, as well as in the nucleus of the solitary tract. Notably, fibers were also present in the gracile nucleus (and to a lesser degree the cuneate nucleus), as well as in the principal trigeminal nucleus, the superior olivary complex, and in pontine nuclei. In the subcortical forebrain, tdTomato$^+$ cells were noted in the anterior olfactory nucleus, the bed nucleus of the stria terminalis, the endopiriform nucleus, the septum and the nucleus of the diagonal band. In the cortex, tdTomato$^+$ cells were generally not found; however, in frontal cortex we observed some tdTomato$^+$ cells in layer 6b immediately superior to the corpus callosum. In addition, tdTomato$^+$ fibers were quite abundant in layer 1a of the frontal cortex, whereas such fibers were very sparse in other cortical regions. Scattered tdTomato$^+$ cells were found in the granule cell layer of the olfactory bulb.

Select peripheral organs and ganglia were surveyed for the presence of tdTomato$^+$ nerve fibers. In glabrous skin, tdTomato$^+$ fibers forming free epidermal nerve endings were abundant (Figure 5A). Notably, although apically directed fibers traversed dermal papillae, we observed no Meissner corpuscle-like endings, as has previously been reported in $Na_V1.8^{Cre}$ mice (Shields et al., 2012). In hairy skin, tdTomato$^+$ circumferential nerve endings around hair follicles were also observed in addition to free nerve endings (Figure 5B). In both glabrous and hairy skin, cutaneous tdTomato$^+$ fibers often but not always colocalized with CGRP immunoreactivity.

Many cells in nodose and jugular ganglia exhibited tdTomato immunoreactivity, as did neurons in the Grüneberg ganglion, a chemo−/thermosensory ganglion in the nose (Figure 6). In skeletal muscle, sparse tdTomato$^+$ fibers were found, while epithelia of the bladder, colon and rectum were richly innervated by tdTomato$^+$ fibers. Similarly, tdTomato$^+$ fibers were abundant in epithelia of both male and female genitalia. In the aortic arch, sparse tdTomato$^+$ fibers were detected, whereas the lamina propria of the olfactory mucosa showed strong innervation by tdTomato$^+$ fibers.

In order to test the utility of the $Na_V1.8^{FlpO}$ strain for intersectional genetic targeting of primary afferent fiber populations, we crossed this line with a $Th^{CreERT2}$ mouse strain and a Cre/Flp-dependent reporter line (Ai65; Figure 7A). In DRGs of these mice, 75.3 ± 1.8% of TH$^+$ neurons showed tdTomato fluorescence, whereas 94.3 ± 1.7% of tdTomato$^+$ cells were TH$^+$, indicating high recombination efficiency and selectivity towards C-LTMRs among primary afferent

10.3389/fnmol.2025.1574219

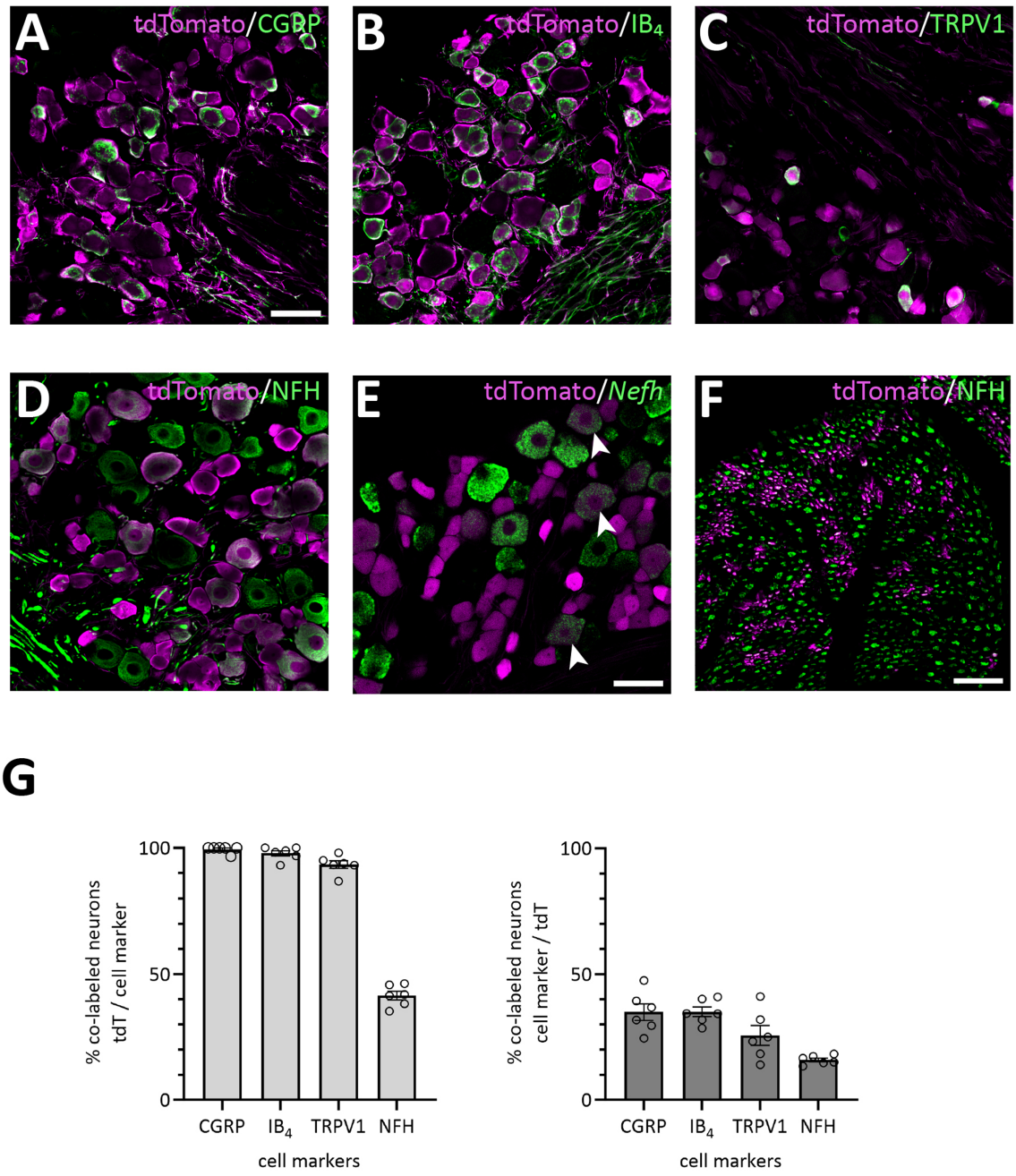


FIGURE 2
Primary afferent populations targeted by the $Na_V1.8^{FlpO}$ mouse line. **(A–E)**, Co-localization of tdTomato-IR with CGRP-IR, IB4 binding, TRPV1-IR, NFH-IR and *Nefh* transcript in lumbar DRGs. Scale bar in A, 50 μm, valid for A-D; scale bar in E, 50 μm. Single optical section, 20x/0.8 objective, pinhole 24 μm **(A–D)** or 32 μm **(E)**. **(F)** Co-localization of tdTomato-IR and NFH-IR in sciatic nerve. Scale bar, 25 μm. Single optical section, 20x/0.8 objective, pinhole 32 μm. **(G)** Quantification of the co-localization of tdTomato with the indicated cell markers. Error bars indicate S.E.M. NFH, CGRP: *n* = 3 mice, 6 DRGs, 1 section per DRG; $IB_4$, TRPV1: *n* = 4 mice, 6 DRGs, 1 section per DRG.

fibers (Figure 7). Importantly, tdTomato fluorescence did not co-localize with nociceptive markers CGRP or IB4, or with the myelinated neuron marker NFH (Supplementary Figure S2). In the lumbar enlargement of the spinal cord of these mice, tdTomato$^+$ processes were evident in a distinct band in the superficial dorsal horn. This band coincided with the dorsal part of the region occupied by neurons expressing the $\gamma$ isoform of protein kinase C (PKC$\gamma$), ventral to the plexus formed by $IB_4$ binding C-fibers (Figure 8A). Notably, tdTomato$^+$ fibers were absent from the medial dorsal horn that receives input from hind paw glabrous skin, and co-localized with VGluT3$^+$ structures. In $Th^{CreERT2}$;$Na_V1.8^{FlpO}$;Ai65 mice, tdTomato fluorescence was restricted to the dorsal roots, tract of Lissauer and ventral lamina II, whereas in $Th^{CreERT2}$;Ai14 mice that target tdTomato to all TH$^+$ cells, various tdTomato$^+$ processes were also observed throughout gray and white matter (Figure 8B). In the hairy skin of $Th^{CreERT2}$; $Na_V1.8^{FlpO}$;Ai65 mice, tdTomato fluorescence was found

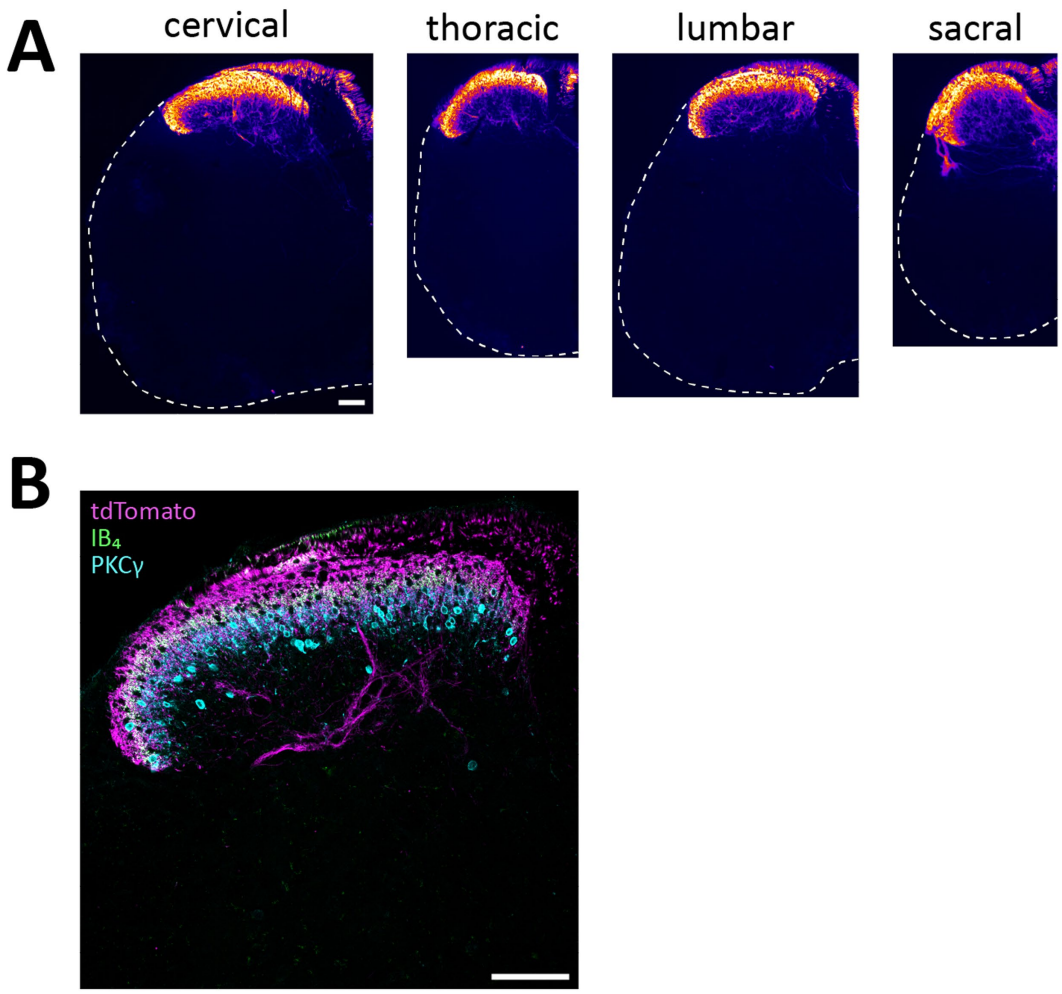


FIGURE 3
tdTomato$^+$ processes in the spinal cord of $Na_V1.8^{FlpO}$; Ai65F mice. **(A)**, distribution of tdTomato$^+$ processes in the spinal cord at different spinal levels. The fluorescence is false-colored to better visualize sparse processes. Dashed lines outline section edges where fluorescence is absent. Scale bar is 100 µm, valid for all panels. Widefield tilescan micrographs obtained using a 20x/0.5 objective. **(B)**, laminar distribution of tdTomato$^+$ fibers in relation to $IB_4$ binding and PKCγ immunolabeling. Single optical section, 20x/0.8 objective, pinhole 27 µm. Scale bar, 100 µm. Images are representative of $n = 4$ mice.

selectively in lanceolate endings surrounding hair follicles, whereas in $Th^{CreERT2}$;Ai14 mice tdTomato fluorescence was also observed in presumed sympathetic fibers. In the brain of $Th^{CreERT2}$; $Na_V1.8^{FlpO}$;Ai65 mice tdTomato$^+$ processes were restricted to the solitary tract, the nucleus of the solitary tract, and, very sparsely, trigeminal structures; other parts of the brain were completely devoid of tdTomato$^+$ processes. By contrast, tdTomato$^+$ fibers and cells showed the expected widespread distribution in $Th^{CreERT2}$; Ai14 mice (Supplementary Figure S3). Thus, using the $Na_V1.8^{FlpO}$ strain affords highly efficient and selective targeting of C-LTMRs while avoiding targeting of central and peripheral catecholaminergic systems.

The ultrastructure of central C-LTMR terminations is contentious, having been described as forming either type I or type II glomeruli in the spinal dorsal horn (Larsson and Broman, 2019; Salio et al., 2021). Such discrepancy could be partly attributed to differences in the markers used for C-LTMR terminals. Here we addressed this issue by creating $Th^{CreERT2}$; $Na_V1.8^{FlpO}$; APEX2 mice, expressing APEX2 in the mitochondrial matrix of C-LTMRs in a Cre-/Flp-dependent manner highly selective for C-LTMRs. In spinal cord from these mice, terminals possessing mitochondria with APEX2 reaction product were commonly found to constitute central terminals of synaptic glomeruli in ventral lamina II (Figure 9). Often irregularly shaped, these terminals exhibited light axoplasm and loosely packed clusters of round and clear synaptic vesicles. In many cases, multiple asymmetric synapses were formed with postsynaptic dendrites. Some of these dendrites contained vesicles and thus presumably originated from inhibitory interneurons (Todd, 1996). Very occasionally, a presynaptic axon was found to form a symmetric synapse onto the central APEX2$^+$ terminal (Figure 9B). Sometimes, the central terminal exhibited more tightly packed vesicle clusters and a scalloped shape, somewhat reminiscent of the central terminals of type I glomeruli (Figure 9C). However, the central terminals of type I glomeruli exhibited a distinctly more electron dense axoplasm and were considerably more tightly packed with vesicles which were of irregular sizes, unlike the more homogenously sized vesicles of APEX2$^+$ terminals. Notably, type I glomeruli were almost always more dorsally located than APEX2$^+$ terminals. Thus, C-LTMRs form type II glomeruli that are readily distinguishable from type I glomeruli formed by $IB_4$ binding non-peptidergic C fiber nociceptors.

10.3389/fnmol.2025.1574219

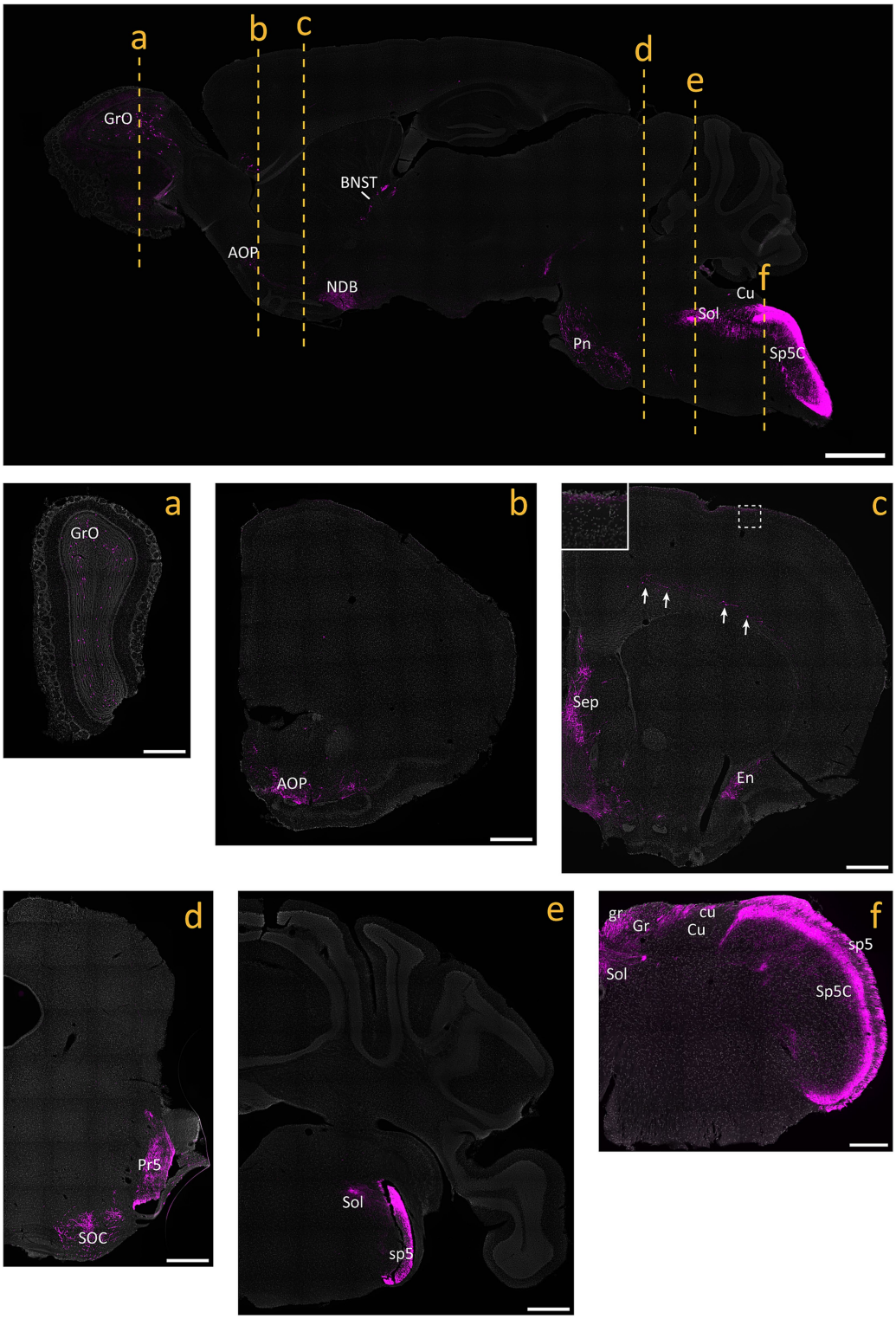


FIGURE 4
tdTomato$^+$ processes and cells in the brain of $Na_V1.8^{FlpO}$; Ai65F mice. Top panel shows a parasagittal brain section. Center and bottom panels show coronal sections obtained at the levels indicated in the parasagittal section. All panels are counterstained with SYTOX Deep Red. Inset in c shows the portion indicated by dashed frame. Arrows indicate tdTomato$^+$ neurons in layer 6 of frontal cortex. AOP, anterior olfactory nucleus, posterior part; BNST, bed nucleus of the stria terminalis; cu, cuneate fascicle; Cu, cuneate nucleus; En, endopiriform nucleus; gr, gracile fascicle; Gr, gracile nucleus; GrO, granular layer of the olfactory bulb; NDB, nucleus of the diagonal band; Pn, pontine nuclei; Pr5, principal sensory trigeminal nucleus; Sep, septal region; SOC, superior olivary complex; Sol, nucleus of the solitary tract; sp5, trigeminal tract; Sp5C, caudal spinal trigeminal nucleus. Scale bar in parasagittal section, 1 mm; scale bars in a-e, 500 µm; scale bar in f, 250 µm. Widefield tilescan micrographs obtained using a 20x/0.5 objective. *n* = 4 mice.

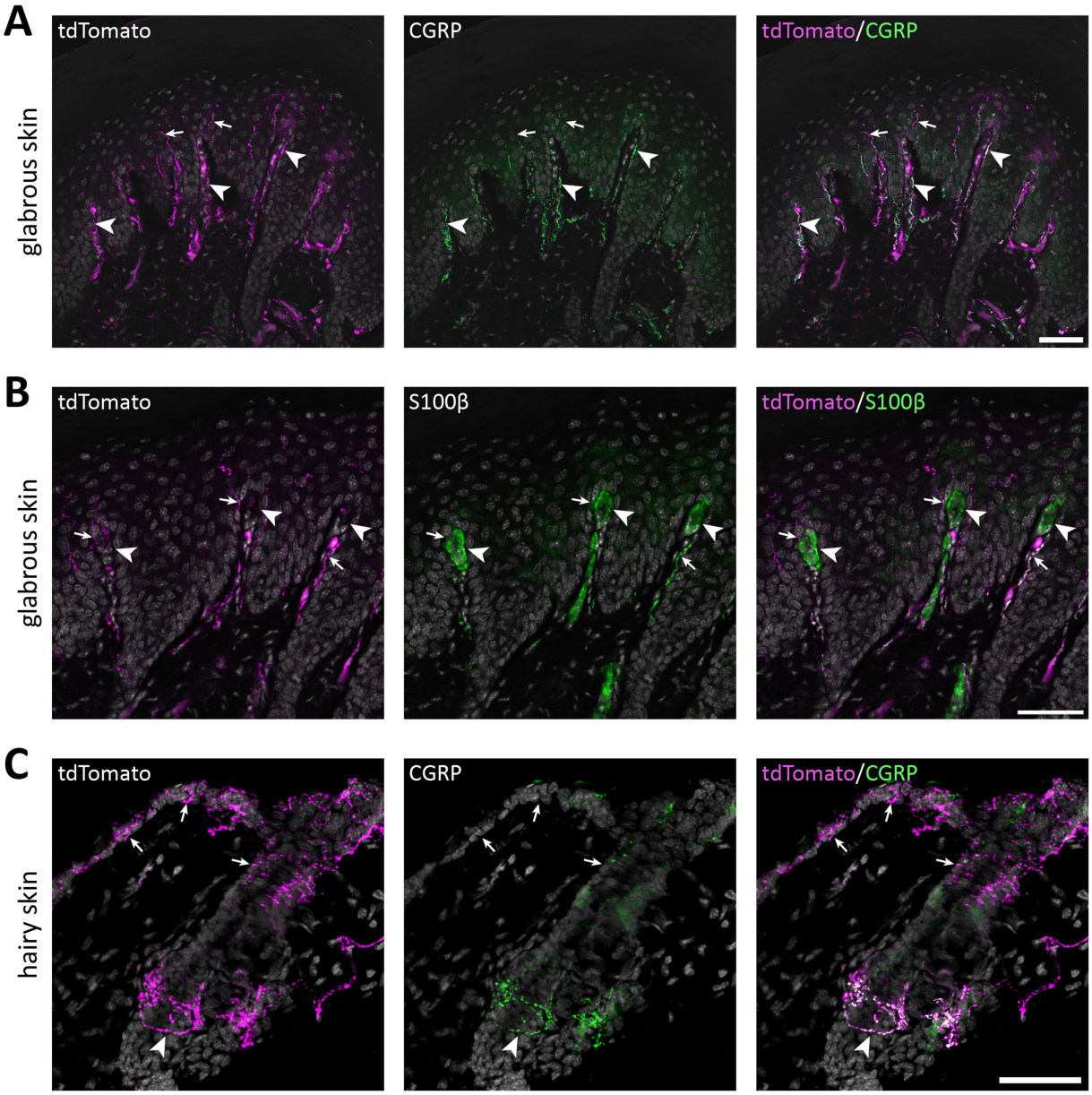


FIGURE 5
tdTomato$^+$ processes in the skin of of $Na_V1.8^{FlpO}$; Ai65F mice. **(A)** tdTomato$^+$ processes and co-localization with CGRP-IR in hind paw glabrous skin. tdTomato$^+$ fibers were frequently CGRP-IR in the dermis, whereas tdTomato$^+$ fibers that lacked CGRP-IR extended into the epidermis. Arrowheads indicate examples of tdTomato$^+$/CGRP$^+$ fibers, and arrows indicate tdTomato$^+$/CGRP$^-$ fibers. Scale bar, 50 µm. Maximum intensity projection of 5 optical sections obtained at 0.47 µm separation using a 20x/0.8 objective with 22 µm pinhole. **(B)** Co-immunolabeling of tdTomato and S100β in hind paw glabrous skin. Whereas tdTomato$^+$ fibers often travelled in dermal papillae, they never formed bundles associated with S100β$^+$ Meissner corpuscles. Arrowheads indicate Meissner corpuscles; arrows indicate examples of tdTomato$^+$ fibers juxtaposed to Meissner corpuscles. Scale bar, 50 µm. Maximum intensity projection of 5 optical sections obtained at 0.47 µm separation using a 20x/0.8 objective with 22 µm pinhole. **(C)** tdTomato$^+$ fibers and co-localization with CGRP in hairy back skin. tdTomato$^+$ fibers formed circumferential CGRP-IR nerve endings around hair follicles (arrowhead), but also free nerve endings in the epidermis that generally lacked CGRP immunoreactivity (arrows). Scale bar, 50 µm. Maximum intensity projection of 25 optical sections obtained at 0.53 µm separation using a 20x/0.8 objective with 24 µm pinhole. All micrographs are counterstained with DAPI. $n$ = 4 mice.

## Discussion

In the present study we have generated and characterized a new knock-in mouse that expresses the recombinase FlpO from the locus of the gene *Scn10a*, that encodes the voltage-gated $Na^+$ channel $Na_V1.8$. We show that this mouse with very high efficiency and selectivity recapitulates the expression of $Na_V1.8$ in primary afferent neurons, and can be used for intersectional targeting of primary afferent fiber populations, as exemplified here by the highly selective targeting of C-LTMRs by combining the new $Na_V1.8^{FlpO}$ mouse, presented in this study, with a $Th^{CreERT2}$ mouse and double recombinase dependent reporter tools.

$Na_V1.8$ was first identified in neurons of DRGs (Akopian et al., 1996) and found to be broadly expressed in nociceptors (Djouhri

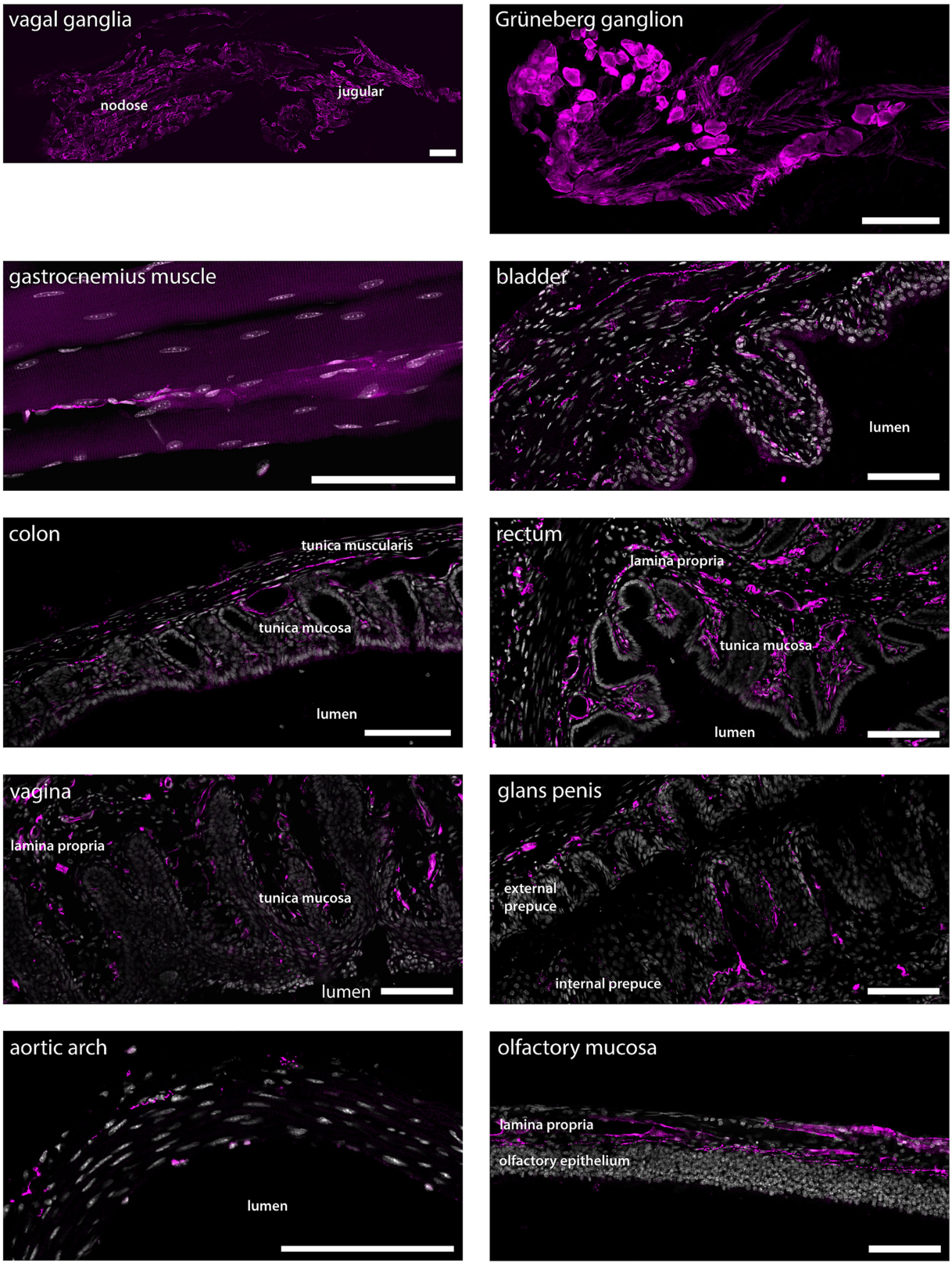


FIGURE 6
tdTomato$^+$ processes and cells in non-dermal peripheral tissue. Scale bars are 100 μm in all panels. Micrographs are single optical sections using a 10x/03 objective and pinhole 24–37 μm for all tissues except for vagal ganglia and aortic arch, the micrographs of which are single optical sections using a 20x/0.8 objective and pinhole 28 μm, and gastrocnemius muscle, which is a maximum intensity projection of 33 optical sections at 0.57 μm separation obtained using a 20x/0.8 objective and 24 μm pinhole. $n$ = 4 mice except genitalia, $n$ = 2 female mice and $n$ = 2 male mice.

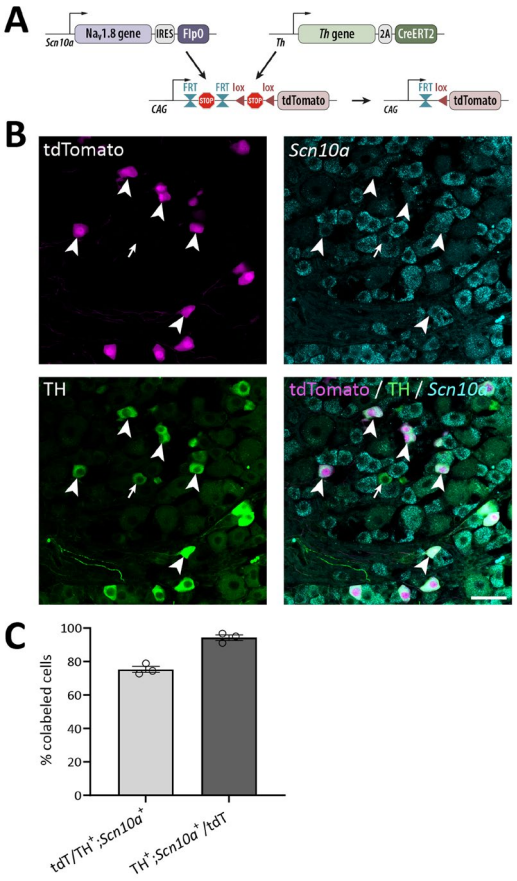


FIGURE 7
Verification of the *Th*$^{CreERT2}$; Na$_V$1.8$^{FlpO}$; Ai65 mouse line. **(A)** Strategy for Cre/Flp-dependent intersectional targeting. Crossing of Ai65 mice with Na$_V$1.8$^{FlpO}$ and *Th*$^{CreERT2}$ mice removes FRT-stop-FRT and (after tamoxifen administration) lox-stop-lox cassettes in cells co-expressing FlpO and CreERT2, enabling transcription of tdTomato in those cells. **(B)** Section of a lumbar DRG subjected to immunolabeling of tdTomato and TH, and to *in situ* hybridization for *Scn10a*. Arrowheads indicate cells triple positive for tdTomato, TH and *Scn10a*. Arrow indicates an example of a TH$^+$/*Scn10a*$^+$ cell that lacks tdTomato expression. Scale bar, 50 μm. Micrographs are single optical sections obtained using a 20x/0.8 objective and 27 μm pinhole. **(C)** Quantification of recombination efficiency with respect to TH$^+$/*Scn10a*$^+$ cells. Note that all TH$^+$ cells were *Scn10a*$^+$ and vice versa. Each data point corresponds to a single DRG section and mouse; *n* = 3 mice. Error bars indicate S.E.M.

et al., 2003). A knock-in/knock-out Na$_V$1.8$^{Cre}$ mouse line was therefore developed (Stirling et al., 2005) which has since been widely used for nociceptor-specific targeting (e.g., Abrahamsen et al., 2008; Daou et al., 2013; Nassar et al., 2004; Lagerström et al., 2011). However, as Na$_V$1.8 is broadly expressed in essentially all nociceptor populations identified, as well as in C-LTMRs (Kupari and Ernfors, 2023; Usoskin et al., 2015), unmasking the roles of these subpopulations of sensory neurons is not possible using the Na$_V$1.8$^{Cre}$ mouse alone. Indeed, genetic markers are generally not selective for a single cell population but also expressed by other cell types, either in the PNS, CNS or non-neural tissue. Using Na$_V$1.8 as one limb of an intersectional targeting approach is useful since it essentially restricts expression to primary nociceptors and C-LTMRs; another gene less specific to the PNS can then be used as a second driver of recombinase expression.

It has been reported that the previously available, widely used Na$_V$1.8$^{Cre}$ mouse line exhibits Cre-dependent recombination not only in nociceptors and C-LTMRs, but also in some A fiber LTMRs, including in nerve endings within Meissner corpuscles (Shields et al., 2012). Here we did not observe any recombined fibers innervating Meissner corpuscles, suggesting that our Na$_V$1.8$^{FlpO}$ mouse does not target any of the two types of rapidly adapting Aβ LTMRs that innervate Meissner corpuscles (Neubarth et al., 2020), in line with the expression of Na$_V$1.8 mostly restricted to Piezo2-poor fibers as observed in transcriptomic studies (Sharma et al., 2020; Usoskin et al., 2015). Still, we did observe a similarly high proportion of recombined neurons that express the A fiber marker NFH as was found with the Na$_V$1.8$^{Cre}$ mouse line (~40%), suggesting that a substantial fraction of fibers exhibiting recombination were myelinated. Some reporter expressing innervation was also found in the dorsal column nuclei as well as in the principal nucleus of the trigeminal nerve, which would speak for FlpO expression in myelinated LTMRs. However, although dorsal column pathways are conventionally viewed as purely involved in low-threshold mechanoreception, they have also been suggested to be involved in visceral nociception, and this could be partly mediated by direct innervation by primary afferent branches (Willis et al., 1999). Nevertheless, although FlpO-dependent recombination very closely followed the expression of the *Scn10a* (Na$_V$1.8) gene, it can from the present observations not

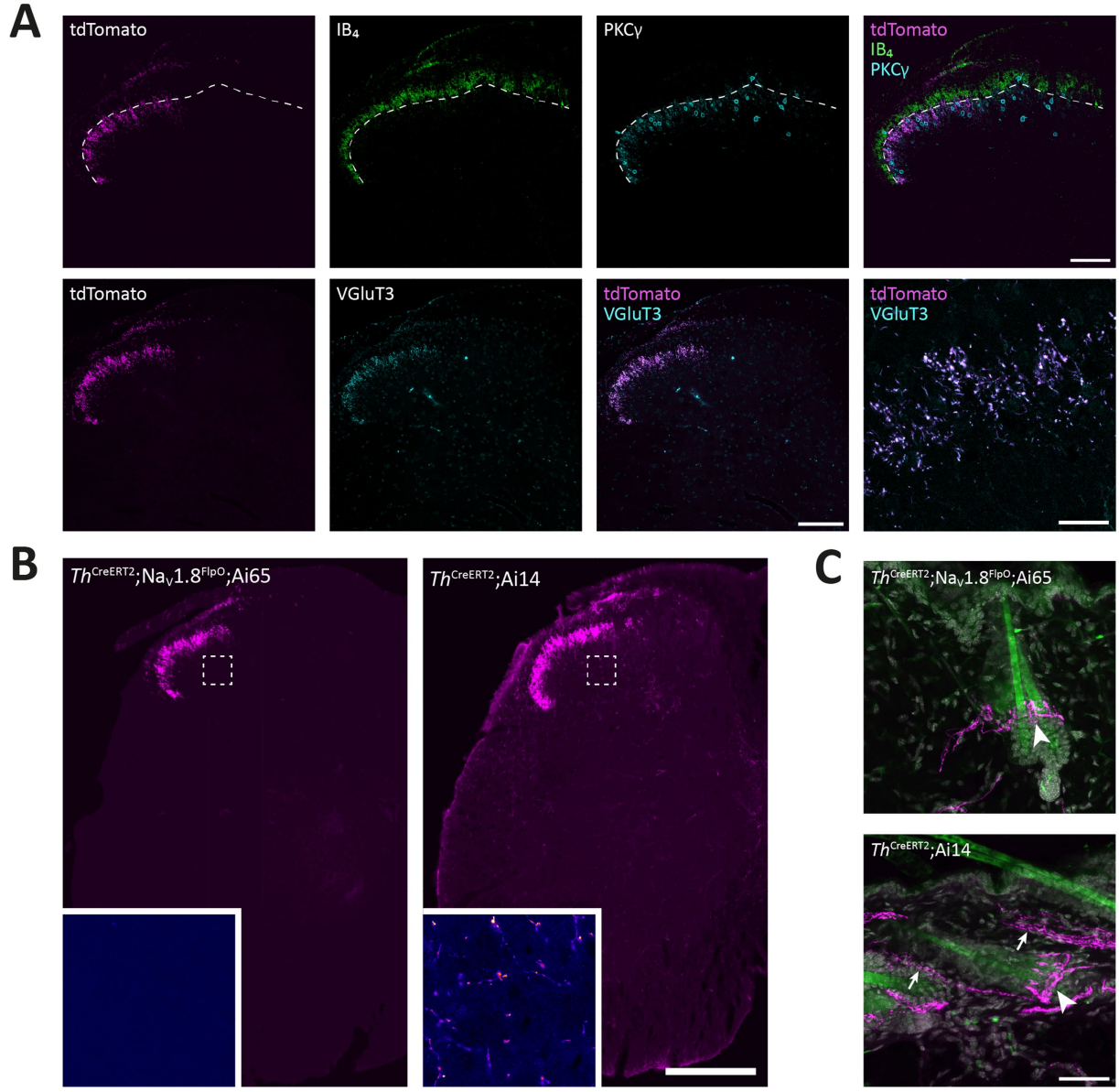


FIGURE 8
Targeting of C-LTMRs in spinal cord and skin of $Th^{CreERT2}$; $Na_V1.8^{FlpO}$; Ai65 mice. **(A)** Distribution of tdTomato$^+$ processes in the superficial dorsal horn of L4 spinal cord with respect to $IB_4$ binding and PKCγ and VGluT3 immunolabeling. Dashed line indicates ventral border of the $IB_4$ plexus. Note that the band of tdTomato$^+$ fibers and endings were almost entirely ventral to this border, and localized to the dorsal portion of the region inhabited by PKCγ neurons. Note that the medial gray matter receiving input from glabrous skin was devoid of tdTomato$^+$ fibers. tdTomato$^+$ processes showed near-complete co-localization with VGluT3 in lamina II. Scale bars are 100 μm except in bottom-rightmost panel, which is 20 μm. Single optical sections obtained using a 20x/0.8 objective and 24 μm pinhole except bottom-rightmost panel, which is a single optical section acquired using a 63x/1.4 objective with 28 μm pinhole. **(B)** Comparison of spinal distribution of tdTomato$^+$ processes in $Th^{CreERT2}$; $Na_V1.8^{FlpO}$; Ai65 versus $Th^{CreERT2}$; Ai14 mice. In the former, tdTomato$^+$ processes were only observed in the superficial dorsal horn as well as in the dorsal root and Lissauer's tract, whereas in $Th^{CreERT2}$; Ai14 mice tdTomato$^+$ processes were present throughout gray and white matter. Insets show magnified false-color views of the regions in the deep dorsal horn indicated by dashed frames. Scale bar, 250 μm. Large views are widefield micrographs obtained using a 20x/0.5 objective; insets are single optical sections obtained using a 40x/1.3 objective and 36 μm pinhole. **(C)** Hairy skin innervation by tdTomato$^+$ fibers in $Th^{CreERT2}$; $Na_V1.8^{FlpO}$; Ai65 versus $Th^{CreERT2}$; Ai14 mice. tdTomato$^+$ lanceolate nerve endings presumably formed by C-LTMRs were found around hair follicles in both mice (indicated by arrowheads). In $Th^{CreERT2}$; Ai14 mice presumed sympathetic nerve fibers were also tdTomato$^+$ (arrows). Images are maximum intensity projections of 26 (upper panel) or 28 (lower panel) optical sections at 1.0 μm separation acquired using a 20x/0.8 objective and 30 μm pinhole. Scale bar, 50 μm.

be excluded that a portion of the fibers showing such recombination were LTMRs.

We surveyed the distribution of recombined nerve fibers in a number of peripheral tissues. In nodose and jugular ganglia, many cells were tdTomato$^+$, in line with previous reports using $Na_V1.8^{Cre}$ mice (Gautron et al., 2011; Stirling et al., 2005), as well as with transcriptomics data (Kupari et al., 2019). Accordingly, we consistently noted extensive innervation of vagal innervation targets, including the bladder wall, intestinal mucosa, and aortic wall. Numerous tdTomato$^+$ fibers were present in the vaginal wall,

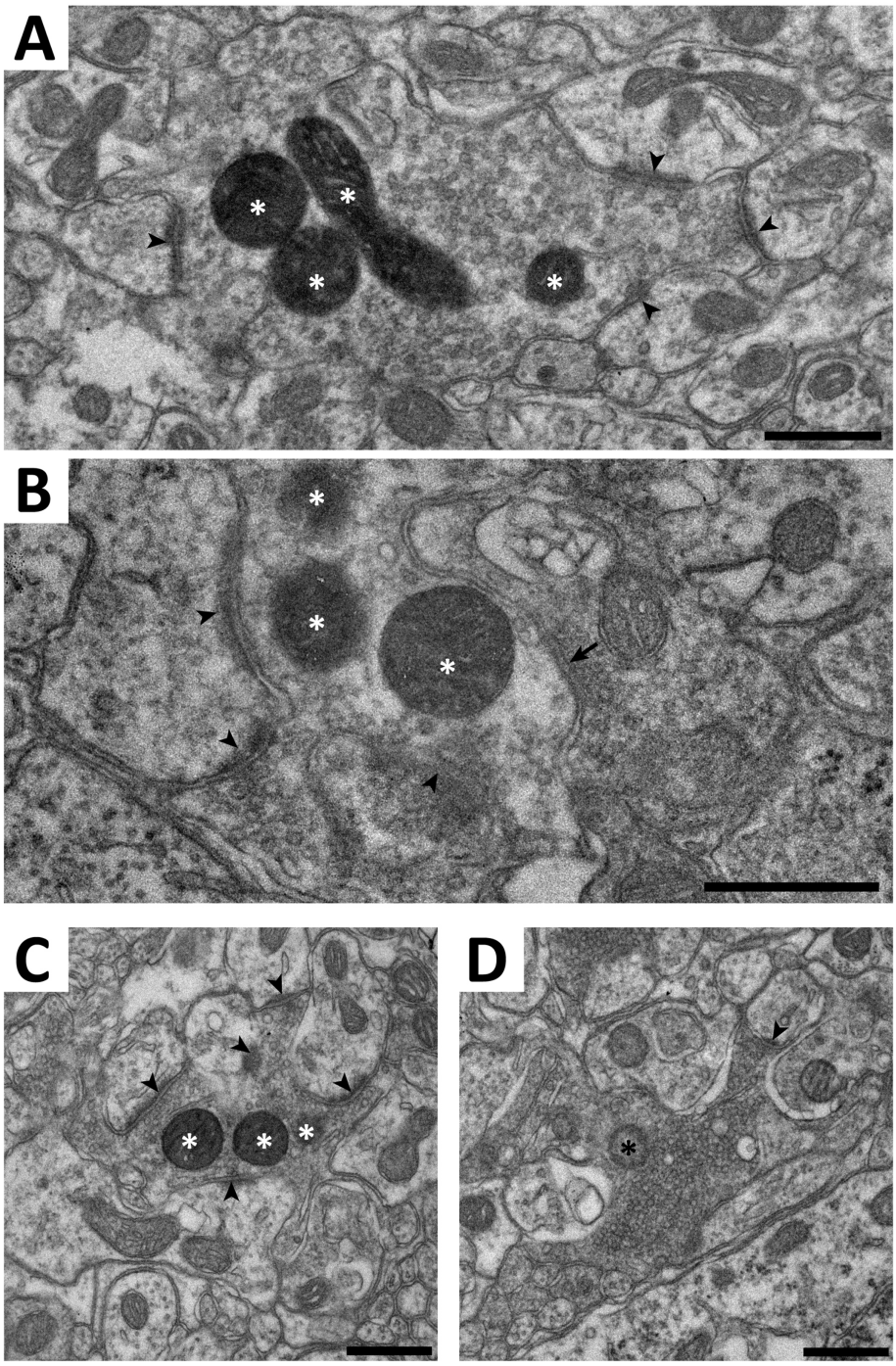


FIGURE 9
Electron microscopy of C-LTMR terminals in spinal cord of *Th*$^{CreERT2}$; Na$_V$1.8$^{FlpO}$;APEX2 mice. **(A–C)** Examples of terminals forming synaptic type II glomeruli in ventral lamina II. White asterisks indicate mitochondria with APEX2 reaction product. Arrowheads indicate asymmetric synapses established by the central APEX2$^+$ terminal onto postsynaptic dendrites. Arrow in **(B)** indicates a symmetric presumed inhibitory synapse formed by a presynaptic axon onto the APEX2$^+$ terminal. **(D)**, a type I glomerulus in mid-dorsal lamina II. The central terminal contains a mitochondrion (black asterisk) lacking APEX2 reaction product. Note the tightly packed synaptic vesicles of variable size, the electron dense axoplasm, and the scalloped shape, compared to the terminals in **(A–C)**. In particular, while the terminal in **(C)** has morphological characteristics resembling those in the terminal in **(D)**, they are much more pronounced in the latter. Scale bars, 500 nm.

including the mucosa and lamina propria, in accordance with the dense innervation by substance P$^+$/CGRP$^+$ fibers previously described (Barry et al., 2017). Similarly, the external and internal prepuces of the glans penis showed dense innervation of tdTomato$^+$ fibers in alignment with recent observations of CGRP$^+$ and TH$^+$ fibers in these structures (Qi et al., 2024a).

A novel finding was the presence of recombined neurons in the Grüneberg ganglion, a little-studied sensory ganglion in the

distal nose. This structure, which has been implicated in the sensation of alarm pheromones and cold (Brechbühl et al., 2008; Schmid et al., 2010), has previously been reported to not show $Na_V1.8$ immunoreactivity (Schmid et al., 2010). Thus, the tdTomato expression found here could reflect either an only weak expression of $Na_V1.8$, or ectopic recombinase expression.

Whereas much attention has been devoted to transcriptomic and neurochemical identification of cutaneous and visceral nociceptor populations, much less is known about nociceptor populations innervating skeletal muscle or other deep somatic tissue (Mense, 2010). Here we found sparse but widespread innervation of recombined fibers in the gastrocnemius muscle, suggesting that the $Na_V1.8^{FlpO}$ mouse can be useful for characterizing of nociceptive muscle afferent fibers.

A somewhat surprising observation was the presence in the CNS of recombined cells and processes that did not originate from primary afferent sources. The presence of $Na_V1.8$ protein or *Scn10a* mRNA in the brain has not been reported in the literature; however, the Allen Brain Atlas does show expression of *Scn10a* mRNA in several regions where we found recombined cells, including the granule cell layer of the olfactory bulb and layer 6 in parts of the frontal cortex. Further investigation is necessary to ascertain whether the reporter expression in our mice is attributed to actual $Na_V1.8$ expression or to ectopic recombination.

We combined the $Na_V1.8^{FlpO}$ line with $Th^{CreERT2}$ mice to test the utility of $Na_V1.8^{FlpO}$ mice in intersectional targeting, and demonstrated that this cross enables efficient and exquisitely selective targeting of C-LTMRs in DRGs without recombination in sympathetic neurons, Merkel cells or in other populations of DRG neurons. Notably, we found very little recombination in the trigeminal system, which is in agreement with the low expression of *Th* observed in C-LTMRs in trigeminal ganglia (Nguyen et al., 2017). A recent study generated a $TAFA4^{CreERT2}$ mouse for targeting of C-LTMRs (Zhang et al., 2024), which selectively express this chemokine (Delfini et al., 2013). However, the $TAFA4^{CreERT2}$ mice also showed recombination in subsets of DRG neurons with nociceptive or myelination markers, as well as in neurons in some regions of the CNS (Zhang et al., 2024). Thus, the intersectional $Th^{CreERT2}$; $Na_V1.8^{FlpO}$ cross used here constitutes a more selective manner of targeting C-LTMRs.

While this manuscript was in preparation, the generation of another $Na_V1.8^{FlpO}$ mouse line was reported (Malapert et al., 2024). The distribution of recombined afferent fibers in spinal cord and peripheral organs in that mouse line is consistent with our observations. Malapert et al. used other reporter mice than those used here, precluding firm comparisons regarding efficiency and selectivity towards $Na_V1.8$ expressing DRG neurons. However, Malapert et al. reported that about 85% of $Scn10a^+$ neurons expressed reporter (efficiency) and that 85% of reporter-positive neurons expressed *Scn10a* (selectivity) in their mouse line, while we observed 97% efficiency and 93% selectivity in this study. Thus, it is possible that our newly generated mouse affords somewhat higher efficiency and selectivity than the previously reported strain.

In conclusion, here we report the generation of a $Na_V1.8^{FlpO}$ mouse line that enables a highly efficient and selective targeting of $Na_V1.8$ expressing primary afferent neurons, as well as hitherto unrecognized small populations of such neurons in the brain. Furthermore, we show that this mouse line enables intersectional targeting of subpopulations of NaV1.8 expressing neurons such as C-LTMRs when combined with suitable Cre driver mice. We anticipate that this mouse line will be a highly useful and versatile tool for the continued exploration of murine sensory systems.

## Data availability statement

The original contributions presented in the study are included in the article/Supplementary material, further inquiries can be directed to the corresponding author.

## Ethics statement

The animal study was approved by Linköpings djurförsöksetiska nämnd. The study was conducted in accordance with the local legislation and institutional requirements.

## Author contributions

JC: Conceptualization, Formal analysis, Investigation, Methodology, Validation, Visualization, Writing – original draft, Writing – review & editing. LK: Formal analysis, Investigation, Methodology, Validation, Writing – original draft, Writing – review & editing. WJ: Conceptualization, Funding acquisition, Methodology, Project administration, Resources, Supervision, Validation, Writing – original draft, Writing – review & editing. ML: Conceptualization, Formal analysis, Funding acquisition, Investigation, Methodology, Project administration, Resources, Supervision, Validation, Visualization, Writing – original draft, Writing – review & editing.

## Funding

The author(s) declare that financial support was received for the research and/or publication of this article. This study was funded by Knut and Alice Wallenberg Foundation, project no. 2019.0047, and the Wallenberg Center for Molecular Medicine (LK and WJ).

## Acknowledgments

We thank Dr. Maria Ntzouni and Dr. Vesa Loitto at the Microscopy Core Facility at the Medical Faculty, Linköping University for technical assistance.

## Conflict of interest

The authors declare that the research was conducted in the absence of any commercial or financial relationships that could be construed as a potential conflict of interest.

## Generative AI statement

The authors declare that no Gen AI was used in the creation of this manuscript.

## Publisher's note



## Supplementary material

The Supplementary material for this article can be found online at: https://www.frontiersin.org/articles/10.3389/fnmol.2025.1574219/full#supplementary-material

**SUPPLEMENTARY FIGURE S1**
tdTomato is not localized to satellite glial cells in DRGs of $Na_V1.8^{FlpO}$; Ai65F mice. Shown is an example view of tdTomato$^+$ neurons, labeled using rabbit anti-RFP, exhibiting enrichment of labeling at the edge of the cells (indicated by arrows). Co-labeling with vimentin as a satellite glial cell marker shows that this enrichment of tdTomato labeling is restricted to neurons and does not localize to adjacent satellite glial cell. SYTOX Deep Red was used as nuclear staining. Scale bar, 10 µm. Images are from a maximum intensity projection of 5 optical sections at 0.260 µm separation acquired using a 40x/1.3 objective and 24 µm pinhole.

**SUPPLEMENTARY FIGURE S2**
Co-localization of tdTomato and cell markers in DRGs from $Th^{CreERT2}$; $Na_V1.8^{FlpO}$; Ai65 mice. Shown are example L3-5 DRG sections labeled for NeuN, CGRP, $IB_4$ binding and NFH. Note lack of co-localization of tdTomato with the nociceptive markers CGRP and $IB_4$ binding, as well as with the A fiber marker NFH. Scale bar is 50 µm, valid for all panels. Images are single optical sections obtained using a 20x/0.8 objective with pinholes of 24 µm (top left panel), 27 µm (top right and bottom left panels), or 32 µm (bottom right panel).

**SUPPLEMENTARY FIGURE S3**
tdTomato$^+$ fibers and cells in the brains of $Th^{CreERT2}$; $Na_V1.8^{FlpO}$; Ai65 and $Th^{CreERT2}$; Ai14 mice. Shown are parasagittal brain sections displaying complete lack of tdTomato fluorescence in the brain of $Th^{CreERT2}$;$Na_V1.8^{FlpO}$; Ai65 mice except for the nucleus of the solitary tracy (Sol) and very sparse fibers in trigeminal areas (top panel), and the expected wide distribution of catecholaminergic structures in $Th^{CreERT2}$; Ai14 mice (bottom panel). Scale bar is 1 mm, valid for both panels. Images are widefield tilescan micrographs obtained using a 20x/0.5 objective.

## References

Abrahamsen, B., Zhao, J., Asante, C. O., Cendan, C. M., Marsh, S., Martinez-Barbera, J. P., et al. (2008). The cell and molecular basis of mechanical, cold, and inflammatory pain. *Science* 321, 702–705. doi: 10.1126/science.1156916

Abraira, V. E., Kuehn, E. D., Chirila, A. M., Springel, M. W., Toliver, A. A., Zimmerman, A. L., et al. (2017). The cellular and synaptic architecture of the mechanosensory dorsal horn. *Cell* 168, 295–310.e19. doi: 10.1016/j.cell.2016.12.010

Akopian, A. N., Sivilotti, L., and Wood, J. N. (1996). A tetrodotoxin-resistant voltage-gated sodium channel expressed by sensory neurons. *Nature* 379, 257–262. doi: 10.1038/379257a0

Barry, C. M., Ji, E., Sharma, H., Beukes, L., Vilimas, P. I., DeGraaf, Y. C., et al. (2017). Morphological and neurochemical differences in peptidergic nerve fibers of the mouse vagina. *J. Comp. Neurol.* 525, 2394–2410. doi: 10.1002/cne.24214

Bonin, R. P., Bories, C., and De Koninck, Y. (2014). A simplified up-down method (SUDO) for measuring mechanical nociception in rodents using von Frey filaments. *Mol. Pain* 10, 1710–1726. doi: 10.1186/1744-8069-10-26

Brechbühl, J., Klaey, M., and Broillet, M.-C. (2008). Grueneberg ganglion cells mediate alarm pheromone detection in mice. *Science* 321, 1092–1095. doi: 10.1126/science.1160770

Bunting, M., Bernstein, K. E., Greer, J. M., Capecchi, M. R., and Thomas, K. R. (1999). Targeting genes for self-excision in the germ line. *Genes Dev.* 13, 1524–1528. doi: 10.1101/gad.13.12.1524

Cong, L., Ran, F. A., Cox, D., Lin, S., Barretto, R., Habib, N., et al. (2013). Multiplex genome engineering using CRISPR/Cas systems. *Science* 339, 819–823. doi: 10.1126/science.1231143

Daigle, T. L., Madisen, L., Hage, T. A., Valley, M. T., Knoblich, U., Larsen, R. S., et al. (2018). A suite of transgenic driver and reporter mouse lines with enhanced brain-cell-type targeting and functionality. *Cell* 174, 465–480.e22. doi: 10.1016/j.cell.2018.06.035

Daou, I., Tuttle, A. H., Longo, G., Wieskopf, J. S., Bonin, R. P., Ase, A. R., et al. (2013). Remote optogenetic activation and sensitization of pain pathways in freely moving mice. *J. Neurosci.* 33, 18631–18640. doi: 10.1523/jneurosci.2424-13.2013

Delfini, M.-C., Mantilleri, A., Gaillard, S., Hao, J., Reynders, A., Malapert, P., et al. (2013). TAFA4, a chemokine-like protein, modulates injury-induced mechanical and chemical pain hypersensitivity in mice. *Cell Rep.* 5, 378–388. doi: 10.1016/j.celrep.2013.09.013

Djouhri, L., Fang, X., Okuse, K., Wood, J. N., Berry, C. M., and Lawson, S. N. (2003). The TTX-resistant Sodium Channel Nav1.8 (SNS/PN3): expression and correlation with membrane properties in rat nociceptive primary afferent neurons. *J. Physiol.* 550, 739–752. doi: 10.1113/jphysiol.2003.042127

Gautron, L., Sakata, I., Udit, S., Zigman, J. M., Wood, J. N., and Elmquist, J. K. (2011). Genetic tracing of Nav1.8-expressing vagal afferents in the mouse. *J. Comp. Neurol.* 519, 3085–3101. doi: 10.1002/cne.22667

Handler, A., and Ginty, D. D. (2021). The mechanosensory neurons of touch and their mechanisms of activation. *Nat. Rev. Neurosci.* 22, 521–537. doi: 10.1038/s41583-021-00489-x

Hoffman, B. U., Baba, Y., Griffith, T. N., Mosharov, E. V., Woo, S. H., Roybal, D. D., et al. (2018). Merkel cells activate sensory neural pathways through adrenergic synapses. *Neuron* 100, 1401–1413.e6. doi: 10.1016/j.neuron.2018.10.034

Huzard, D., Martin, M., Maingret, F., Chemin, J., Jeanneteau, F., Mery, P. F., et al. (2022). The impact of C-tactile low-threshold mechanoreceptors on affective touch and social interactions in mice. *Sci. Adv.* 8:eabo7566. doi: 10.1126/sciadv.abo7566

Kaczmarczyk, L., Reichenbach, N., Blank, N., Jonson, M., Dittrich, L., Petzold, G. C., et al. (2021). Slc1a3-2A-CreERT2 mice reveal unique features of Bergmann glia and augment a growing collection of Cre drivers and effectors in the 129S4 genetic background. *Sci. Rep.* 11:5412. doi: 10.1038/s41598-021-84887-2

Kupari, J., and Ernfors, P. (2023). Molecular taxonomy of nociceptors and pruriceptors. *Pain* 164, 1245–1257. doi: 10.1097/j.pain.0000000000002831

Kupari, J., Häring, M., Agirre, E., Castelo-Branco, G., and Ernfors, P. (2019). An atlas of vagal sensory neurons and their molecular specialization. *Cell Rep.* 27, 2508–2523.e4. doi: 10.1016/j.celrep.2019.04.096

Lagerström, M. C., Rogoz, K., Abrahamsen, B., Lind, A.-L., Ölund, C., Smith, C., et al. (2011). A sensory subpopulation depends on vesicular glutamate transporter 2 for mechanical pain, and together with substance P, inflammatory pain. *Proc. Natl. Acad. Sci.* 108, 5789–5794. doi: 10.1073/pnas.1013602108

Larsson, M., and Broman, J. (2019). Synaptic organization of VGLUT3 expressing low-threshold mechanosensitive C fiber terminals in the rodent spinal cord. *eNeuro* 6:ENEURO.0007-19.2019. doi: 10.1523/eneuro.0007-19.2019

Larsson, M., and Nagi, S. S. (2022). Role of C-tactile fibers in pain modulation: animal and human perspectives. *Curr. Opin. Behav. Sci.* 43, 138–144. doi: 10.1016/j.cobeha.2021.09.005

Li, C.-L., Li, K.-C., Wu, D., Chen, Y., Luo, H., Zhao, J.-R., et al. (2015). Somatosensory neuron types identified by high-coverage single-cell RNA-sequencing and functional heterogeneity. *Cell Res.* 26, 83–102. doi: 10.1038/cr.2015.149

Li, L., Rutlin, M., Abraira Victoria, E., Cassidy, C., Kus, L., Gong, S., et al. (2011). The functional organization of cutaneous low-threshold mechanosensory neurons. *Cell* 147, 1615–1627. doi: 10.1016/j.cell.2011.11.027

Löken, L. S., Wessberg, J., Morrison, I., McGlone, F., and Olausson, H. (2009). Coding of pleasant touch by unmyelinated afferents in humans. *Nat. Neurosci.* 12, 547–548. doi: 10.1038/nn.2312

Madisen, L., Zwingman, T. A., Sunkin, S. M., Oh, S. W., Zariwala, H. A., Gu, H., et al. (2010). A robust and high-throughput Cre reporting and characterization system for the whole mouse brain. *Nat. Neurosci.* 13, 133–140. doi: 10.1038/nn.2467

Malapert, P., Robert, G., Brunet, E., Chemin, J., Bourinet, E., and Moqrich, A. (2024). A novel Na<sub>v</sub>1.8-FLPo driver mouse for intersectional genetics to uncover

the functional significance of primary sensory neuron diversity. *iScience* 27:109396. doi: 10.1016/j.isci.2024.109396

Mense, S. (2010). "Peripheral mechanisms of muscle pain: response behavior of muscle nociceptors and factors eliciting local muscle pain" in Muscle pain: Understanding the mechanisms. eds. S. Mense and R. D. Gerwin (Berlin: Springer), 49–103.

Nassar, M. A., Stirling, L. C., Forlani, G., Baker, M. D., Matthews, E. A., Dickenson, A. H., et al. (2004). Nociceptor-specific gene deletion reveals a major role for Nav1.7 (PN1) in acute and inflammatory pain. *Proc. Natl. Acad. Sci.* 101, 12706–12711. doi: 10.1073/pnas.0404915101

Neubarth, N. L., Emanuel, A. J., Liu, Y., Springel, M. W., Handler, A., Zhang, Q., et al. (2020). Meissner corpuscles and their spatially intermingled afferents underlie gentle touch perception. *Science* 368:abb2751. doi: 10.1126/science.abb2751

Nguyen, M. Q., Wu, Y., Bonilla, L. S., von Buchholtz, L. J., and Ryba, N. J. P. (2017). Diversity amongst trigeminal neurons revealed by high throughput single cell sequencing. *PLoS One* 12:e0185543. doi: 10.1371/journal.pone.0185543

Olausson, H., Lamarre, Y., Backlund, H., Morin, C., Wallin, B. G., Starck, G., et al. (2002). Unmyelinated tactile afferents signal touch and project to insular cortex. *Nat. Neurosci.* 5, 900–904. doi: 10.1038/nn896

Qi, L., Iskols, M., Greenberg, R. S., Xiao, J. Y., Handler, A., Liberles, S. D., et al. (2024a). Krause corpuscles are genital vibrotactile sensors for sexual behaviours. *Nature* 630, 926–934. doi: 10.1038/s41586-024-07528-4

Qi, L., Iskols, M., Shi, D., Reddy, P., Walker, C., Lezgiyeva, K., et al. (2024b). A mouse DRG genetic toolkit reveals morphological and physiological diversity of somatosensory neuron subtypes. *Cell* 187, 1508–1526.e16. doi: 10.1016/j.cell.2024.02.006

Salio, C., Aimar, P., Malapert, P., Moqrich, A., and Merighi, A. (2021). Neurochemical and ultrastructural characterization of unmyelinated non-peptidergic C-nociceptors and C-low threshold mechanoreceptors projecting to lamina II of the mouse spinal cord. *Cell. Mol. Neurobiol.* 41, 247–262. doi: 10.1007/s10571-020-00847-w

Schmid, A., Pyrski, M., Biel, M., Leinders-Zufall, T., and Zufall, F. (2010). Grueneberg ganglion neurons are finely tuned cold sensors. *J. Neurosci.* 30, 7563–7568. doi: 10.1523/jneurosci.0608-10.2010

Sharma, N., Flaherty, K., Lezgiyeva, K., Wagner, D. E., Klein, A. M., and Ginty, D. D. (2020). The emergence of transcriptional identity in somatosensory neurons. *Nature* 577, 392–398. doi: 10.1038/s41586-019-1900-1

Shields, S. D., Ahn, H. S., Yang, Y., Han, C., Seal, R. P., Wood, J. N., et al. (2012). Nav1.8 expression is not restricted to nociceptors in mouse peripheral nervous system. *Pain* 153, 2017–2030. doi: 10.1016/j.pain.2012.04.022

Stirling, C. L., Forlani, G., Baker, M. D., Wood, J. N., Matthews, E. A., Dickenson, A. H., et al. (2005). Nociceptor-specific gene deletion using heterozygous NaV1.8-Cre recombinase mice. *Pain* 113, 27–36. doi: 10.1016/j.pain.2004.08.015

Todd, A. J. (1996). GABA and glycine in synaptic glomeruli of the rat spinal dorsal horn. *Eur. J. Neurosci.* 8, 2492–2498. doi: 10.1111/j.1460-9568.1996.tb01543.x

Usoskin, D., Furlan, A., Islam, S., Abdo, H., Lönnerberg, P., Lou, D., et al. (2015). Unbiased classification of sensory neuron types by large-scale single-cell RNA sequencing. *Nat. Neurosci.* 18, 145–153. doi: 10.1038/nn.3881

Willis, W. D., Al-Chaer, E. D., Quast, M. J., and Westlund, K. N. (1999). A visceral pain pathway in the dorsal column of the spinal cord. *Proc. Natl. Acad. Sci.* 96, 7675–7679. doi: 10.1073/pnas.96.14.7675

Wu, S., Ying, G., Wu, Q., and Capecchi, M. R. (2008). A protocol for constructing gene targeting vectors: generating knockout mice for the cadherin family and beyond. *Nat. Protoc.* 3, 1056–1076. doi: 10.1038/nprot.2008.70

Zhang, Q., Lee, W.-C. A., Paul, D. L., and Ginty, D. D. (2019). Multiplexed peroxidase-based electron microscopy labeling enables simultaneous visualization of multiple cell types. *Nat. Neurosci.* 22, 828–839. doi: 10.1038/s41593-019-0358-7

Zhang, D., Turecek, J., Choi, S., Delisle, M., Pamplona, C. L., Meltzer, S., et al. (2024). C-LTMRs evoke wet dog shakes via the spinoparabrachial pathway. *Science* 386, 686–692. doi: 10.1126/science.adq8834